Liping Zeng ✉
Zihao Wan
Gang Li
Ruqi Ding
Guoliang Hu
Hongen Niu

https://doi.org/10.21278/TOF.493062123
ISSN 1333-1124
eISSN 1849-1391

DESIGN AND ELECTROMAGNETIC FIELD ANALYSIS OF A MOMENT OF INERTIA ADJUSTMENT DEVICE BASED ON ELECTROMAGNETIC CONTROL

Summary

The vibration frequency characteristics of a rotor system are directly related to the moment of inertia of the system. In this paper, a moment of inertia adjustment device based on electromagnetic control is proposed to adjust the frequency characteristics of the rotor system and better reduce vibration by changing the moment of inertia. First, the finite element simulation model is established, and the electromagnetic field of the electromagnetic control unit in the device is analysed. The influence of materials and parameters of the main parts on the electromagnetic field is discussed. Then, the validity of the finite element simulation results for the electromagnetic control unit is tested by experiments. Finally, the variation of the displacement and force of the moving mass and the changes with speed in the device's moment of inertia under different magnitudes of electrical current are analysed. The results show that the proposed moment of inertia adjustment device can be used to finely adjust the moment of inertia, which enables better control of vibrations in rotor systems.

Key words: *moment of inertia adjustment device; electromagnetic field; mechanical model; finite element simulation*

1. Introduction

A flywheel is a common mechanical device that is usually applied for alleviating speed fluctuations, energy storage, or suppressing vibration in machines. Due to its high efficiency, low pollution, simple maintenance, and other advantages, it is widely applied in advanced technical fields, including aerospace, vehicles, and energy engineering [1–6]. In order to achieve small fluctuations in angular velocity, a flywheel with a large moment of inertia is required. However, a large moment of inertia can make it difficult to start an engine or other rotor systems [7]. In general, the vibrations and speed fluctuations of a mechanical system become more severe as the speed increases. A variable inertia flywheel is a device that can effectively solve this problem. Researchers have conducted extensive research on variable

inertia flywheels. In 1979, the American scholar Ullman [8] proposed the concept of a variable inertia flywheel and a fly ball governor. Van de [9] proposed a fluid variable inertia flywheel that is divided into two chambers through movable pistons; one chamber is filled with fluid, and the other chamber is in contact with the air. The size of the fluid chamber changes through the movement of the piston; this can adjust the moment of inertia of the flywheel. Dugas [10] acquired the variable inertia of the flywheel through the valve control of the fluid flow. The variable inertia of the flywheel in reference [11] was acquired by filling and draining. By controlling the fluid in the chamber, the variable inertia flywheel can minimize the variations in engine speed caused by changes in the power load; it, however, becomes complicated due to the filling and control of the fluid.

The above method of achieving the variable moment of inertia involves changing the mass of the flywheel. However, the actual structure implemented in this way will be very complex and difficult to operate. The research into the variable inertia flywheel mainly focuses on changing the distance from the movable mass in the flywheel to the centre of rotation. Xu et al. [12], developed a two-terminal mass-based vibration absorber with a variable moment of inertia achieved by the motion of sliders embedded in a hydraulically driven flywheel for passive vehicle suspension. The vibration absorber has better stability and a faster response speed compared to the flywheel with constant inertia. Kondoh et al. [13] proposed a new type of flywheel energy storage system in which the moment of inertia is controlled actively for charging and discharging without a power electronic interface while the rotational speed is maintained almost constant. In the field of a hydraulic drive, the effects of the variable inertia flywheel on the hydraulic motor speed fluctuations were compared with those of the fixed inertia flywheel [14]. The results show that the variable inertia generated by the variable inertia flywheel can better reduce the hydraulic motor speed fluctuations in response to the changes in the excitation inputs. To improve the speed stability of a diesel generator against loading impact, Zhang et al. [15] filed a patent application for a variable inertia shock absorber with an inertia ring and a rubber ring mounted on a hub. Their design can be used for automobile internal combustion engines. Su et al. [16] designed a hybrid power system with a variable inertia flywheel, developed kinematics and dynamics equations of the system, determined the relationship between the speed and torque of each component, and used the ADVISOR software to determine the necessary output speed and torque of the vehicle under various operating conditions. Harrowell [17] presented a new concept of elastic flywheel using vulcanized rubber based on the principle of material strain. The concept exploits the nonlinear expansion of an elastomer ring together with its variable moment of inertia. Recently, Chen et al. [18] proposed a vibration energy harvester for bicycle based on a directional variable inertia flywheel and a coaxial mechanical motion rectifier

The moment of inertia of a rotor system directly affects its natural frequency characteristics, vibration characteristics, and transmission performance. The technology of a variable moment of inertia has great potential for reducing torque and speed fluctuations in mechanical systems. However, until now, only a few articles on the application of the variable inertia based on electromagnetic control have been reported. There is a need to explore the realization of the variable moment of inertia based on electromagnetic control. In this study, an electromagnetic control unit is introduced into a flywheel structure. Thus, a new type of easily detachable device for adjusting the moment of inertia is proposed. The electromagnetic field characteristics of the structure are basically determined by the material properties, geometry, and rotating speed of the rotor. The finite element simulation analysis of the electromagnetic field characteristics of the electromagnetic control unit is carried out; the results are verified by experiments. The influence of different parameters on the electromagnetic field and variable inertia is studied as well.

2. The structure and working principle of the moment of inertia adjustment device

Figure 1 shows the structure of the moment of inertia adjustment device, which mainly consists of a flywheel mounting and four electromagnetic control units. Each electromagnetic control unit consists of two permanent magnets, a coil, a spring, a long sleeve, a short sleeve, and a fixing plate. The coil is wound around the permanent magnet 1, and fixed in the long sleeve using adhesive. The permanent magnet 2 is fixed in the short sleeve using adhesive. The short sleeve and the fixing plate are connected by a spring. Besides that, the two permanent magnets are installed in the long sleeve with the same pole opposite each other. They are then placed in the groove of the flywheel mounting and fixed through the cover plate. When the device rotates, the radial position of the permanent magnet 2 and the short sleeve can be adjusted by changing the coil current under the action of centrifugal force, spring force, and electromagnetic force. In this way, different moments of inertia can be obtained.

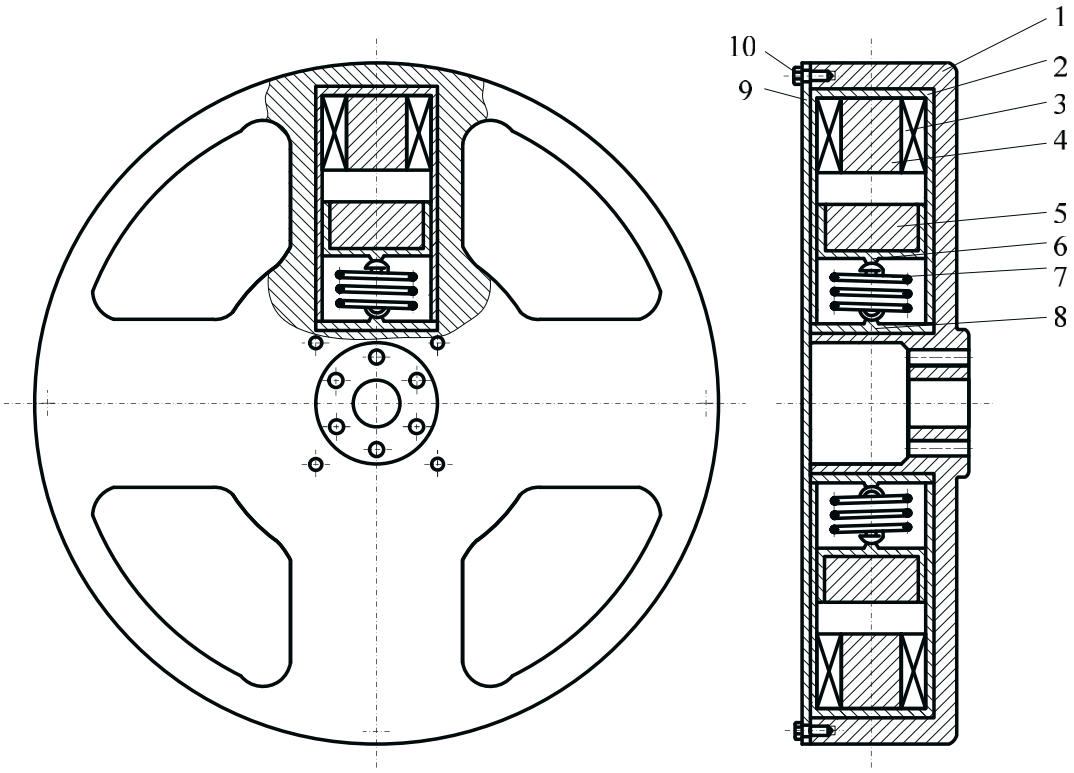

1- Flywheel mounting; 2-Long sleeve; 3-Coil; 4- Permanent magnet 1; 5- Permanent magnet 2; 6- Short sleeve; 7- Spring; 8- Fixing plate; 9- Cover plate; 10- Screw

Fig. 1 Schematic diagram of the structure of the moment of inertia adjustment device

3. Finite element simulation analysis of the electromagnetic control units

Permanent magnet 2 and the short sleeve are subjected to electromagnetic force during motion. Electromagnetic field characteristics of the electromagnetic control unit are analysed using the finite element method in order to determine the influence of some parameters, such as the material of the sleeve and the heights of each permanent magnet, on the magnitude of electromagnetic force and magnetic induction distribution. A two-dimensional axisymmetric model of the electromagnetic control unit is established, as shown in Fig. 2. The flywheel mounting is made of 6061 aluminium alloy, a non-magnetic material, and is not taken into account. The two permanent magnets are all made of N48, a strong neodymium-iron-boron magnet. The material of the coil is copper. The other parts are air regions. The main parameters for finite element analysis are listed in Table. 1.

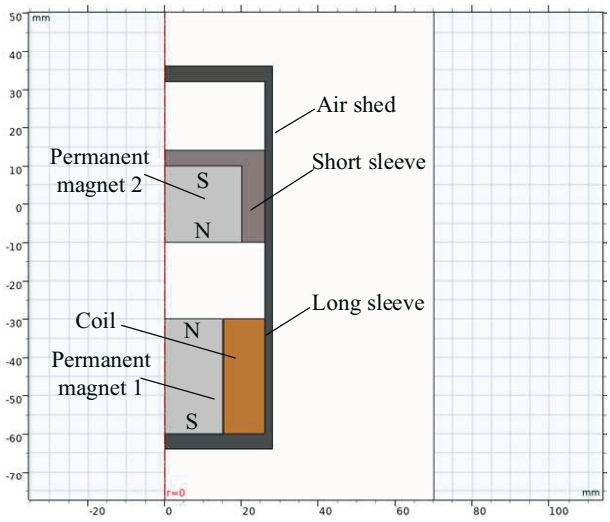

Fig. 2 A two-dimensional axisymmetric model of electromagnetic control units

Table 1 Main parameters of the finite element analysis model

Parameter	Numerical value	Parameter	Numerical value
Permanent magnet 1 diameter d_1 /mm	30	Coil diameter d_5 /mm	0.6
Permanent magnet 2 diameter d_2 /mm	40	Permanent magnet remanence Br /T	1.43
Short sleeve outside diameter d_3 /mm	54	Air permeability μ_0 /(H/mm)	1.25×10^{-8}
Long sleeve outside diameter d_4 /mm	58	Coercive force H_c /(kA/mm)	10.34

Select the residual magnet model under the Ampere's law option for permanent magnets, and set parameters such as the coil current I and the number of turns N. As shown in Fig. 3, triangle elements are used to divide the grid. For the area between the coil and the permanent magnet 1, the boundary layer option is used to encrypt the grid. The maximum and minimum sizes of the grid element are 5 mm and 0.02 mm, respectively. Permanent magnet 2 and the short sleeve, which are the moving parts, are set to move radially. The initial position (air gap) relative to the permanent magnet 1 is δ_0=20 mm.

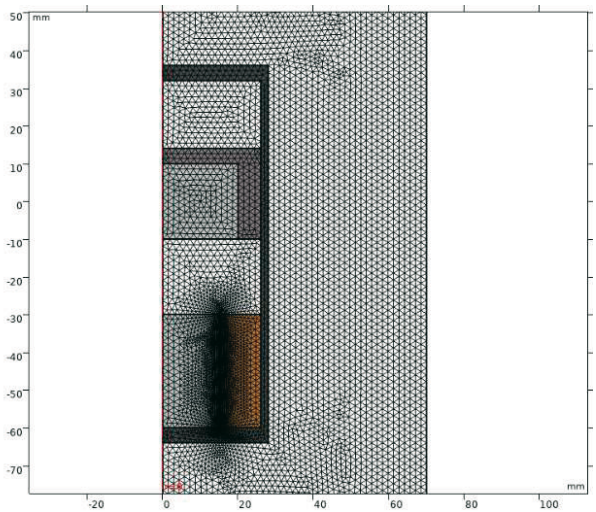

Fig. 3 Grid division of the finite element model

3.1 Effect of the sleeve material on electromagnetic force and magnetic induction distribution

To analyse the influence of structural materials on the magnetic fields in electromagnetic control units, four analysis plans are devised by selecting long sleeves and short sleeves as different materials. The four analysis plans are listed in Table 2. In addition, the lengths of permanent magnet 1 and permanent magnet 2 are set to h_1=30 mm and h_2=20 mm, respectively. Taking I=2 A, N=800, δ=1 mm, the electromagnetic field finite element simulation for the four analysis plans is carried out.

Figure 4 shows the magnetic field line distribution and the cloud diagram of the magnetic induction intensity of the electromagnetic control units. It can be seen that there are significant differences in the magnetic field line distribution, magnetic induction intensity distribution, and electromagnetic force variation among the four plans. The magnetic field lines start from the N pole of the permanent magnet, pass through the air, and return to the S pole of the permanent magnet to form a closed loop. The magnetic fields of the two permanent magnets are in opposite directions. The magnetic field lines are more densely distributed in cast iron than those in stainless steel, and the magnetic resistance of cast iron is much lower than that of stainless steel. In addition, the magnetic induction intensity on a permanent magnet exhibits a characteristic of being large at both ends and small in the middle, with a relatively uniform distribution. The maximum value occurs at the point where the structural shape changes. This is because the magnetic field lines of the permanent magnet converge from the two poles, resulting in an increase in the magnetic induction intensity at both ends of the permanent magnet. Due to the strongest interaction between the magnetic field of the permanent magnet and the magnetic field generated by the coil at the intersection of permanent magnet 1 and the coil, the magnetic field of the permanent magnet and the magnetic field generated by the coil have the strongest superposition effect.

Table 2 Four plans for selecting sleeve materials

Sleeves	Materials			
	Plan A	Plan B	Plan C	Plan D
Long sleeve	Cast iron	Stainless steel	Cast iron	Stainless steel
Short sleeve	Stainless steel	Cast iron	Cast iron	Stainless steel

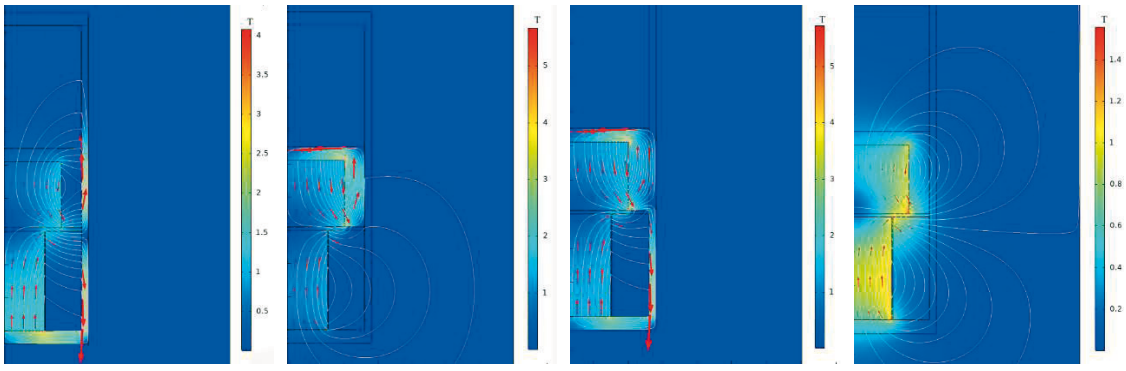

(a) Plan A (b) Plan B (c) Plan C (d) Plan D

Fig. 4 Magnetic field line distribution and magnetic induction intensity cloud diagram of the electromagnetic control units in the four different plans

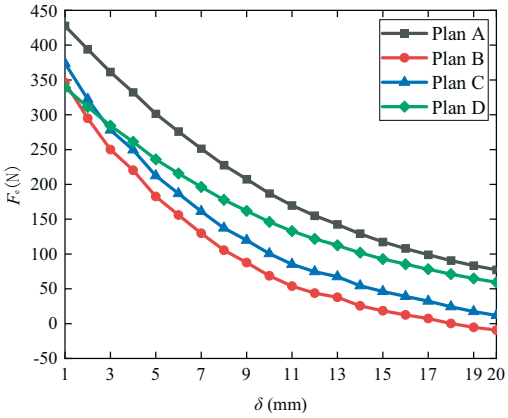

Fig. 5 The variations in the electromagnetic force with the air gap in the four different plans

Figure 5shows the relationship between the electromagnetic force F_e of the electromagnetic control unit and the air gap δ. In the four plans, the electromagnetic force decreases with an increase in the air gap. Plan A has a slower decreasing trend and more numerical advantages; therefore, plan A is selected, that is, cast iron is used for the long sleeve and stainless steel is used for the short sleeve.

3.2 Effect of the permanent magnet 2 height on the electromagnetic force and magnetic induction distribution

Taking h_1=30 mm, I=2 A, and N=800, the electromagnetic field analysis of the electromagnetic control units is carried out with different heights of permanent magnet 2. Figure 6 shows the magnetic field line distribution and magnetic induction intensity cloud diagram, and Figure 7 the variation in the electromagnetic force with the current at δ=1 mm. The simulation results show that the distribution of the magnetic field lines and the magnetic induction intensity is approximately the same at different heights of permanent magnet 2, but there are differences in numerical values. Since the magnetic lines of force always preferentially pass through the places with small magnetic resistance, the magnetic lines of force are densely distributed in the long sleeve, and the magnetic induction intensity at the bottom and the side of the long sleeve is generally greater than that on the permanent magnet. As shown in Fig. 7, the stronger the current, the greater the electromagnetic force will be.

Figure 8 shows the variation in the electromagnetic force with changes in the air gap. The decreasing trend of the electromagnetic force becomes less marked as the air gap increases. In addition, the generated electromagnetic force increases as the heights of permanent magnet 2 increase.

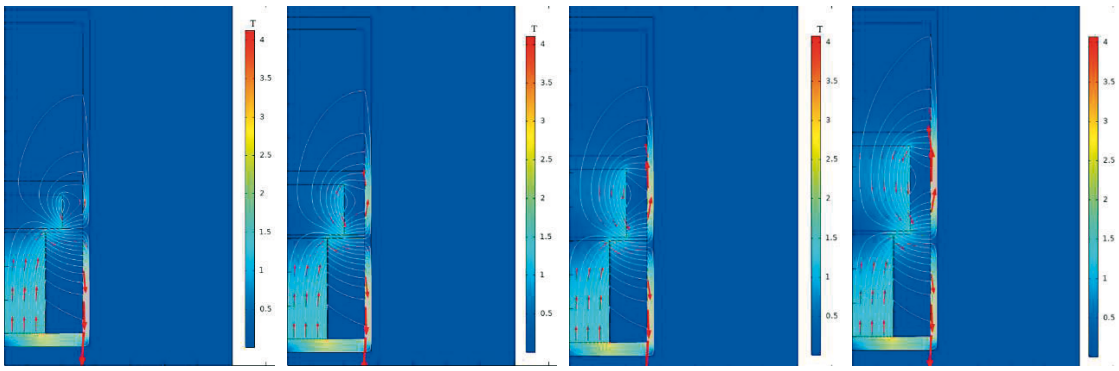

(a) h_2=10 mm (b) h_2=15 mm (c) h_2=20 mm (d) h_2=25 mm

Fig. 6 Magnetic field line distribution and magnetic induction intensity cloud diagram of an electromagnetic control unit for different heights of the permanent magnet 2

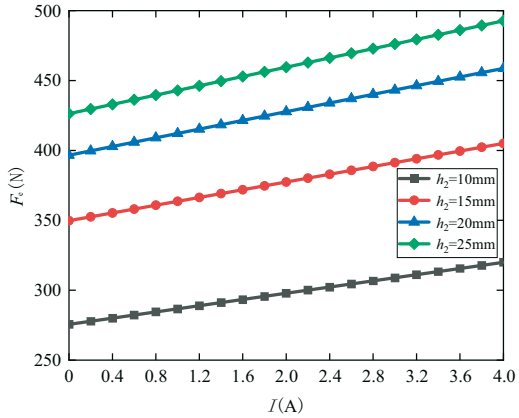

Fig. 7 The variation in the electromagnetic force with current for different heights of the permanent magnet 2

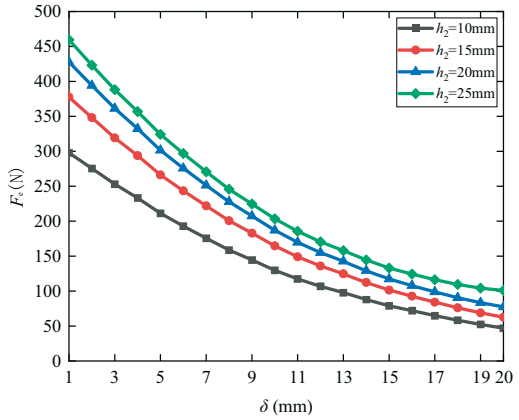

Fig. 8 The variation in the electromagnetic force with air gap for different heights of the permanent magnet 2

3.3 Effect of heights of the permanent magnet 1 on the electromagnetic force and magnetic induction distribution

Taking h_2=20 mm and I=2 A, the electromagnetic field analysis of the electromagnetic control units is carried out at different heights of the permanent magnet 1.Since the radial distance between the permanent magnet 1 and the long sleeve remains unchanged, the coil cross-sectional area increases with the increase in the heights of the permanent magnet 1and the number of turns in the coil also increases. The number of turns corresponding to the different heights of the permanent magnet 1 is 500 turns (20 mm), 700 turns (25 mm), 800 turns (30 mm), 900 turns (35 mm), and 1000 turns (40 mm), respectively.

Figure 9 shows the magnetic field line distribution and the cloud diagram of magnetic induction intensity of the electromagnetic control unit with different heights of the permanent magnet 1 at δ=1 mm. The variation in the electromagnetic force with current is shown in Fig. 10. As one can see, the distribution of magnetic field lines and magnetic induction intensity are approximately the same for different heights of the permanent magnet 1. The distribution of magnetic field lines is relatively dense in long sleeves, and the magnetic induction intensity is greater in these areas than that on permanent magnets. As the magnitude of electrical current increases, the electromagnetic force increases linearly. The greater the height of the permanent magnet 1, the stronger the electromagnetic force. In addition, as shown in Fig. 11, the electromagnetic force decreases as the air gap increases, and the trend of electromagnetic force variation at different heights of the permanent magnet 1 is very similar.

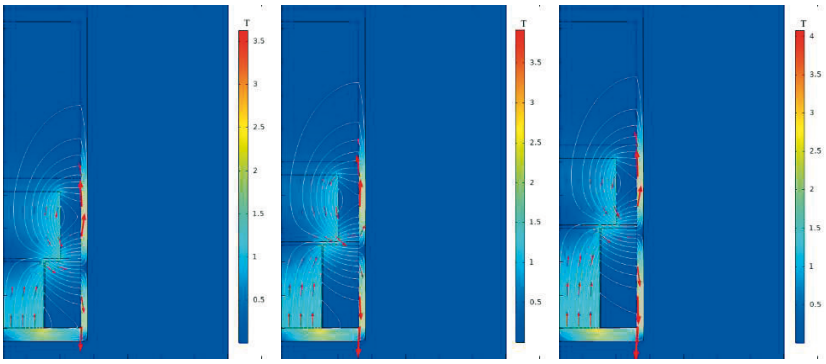

(a) h_1=20 mm (b) h_1=25 mm (c) h_1=30 mm

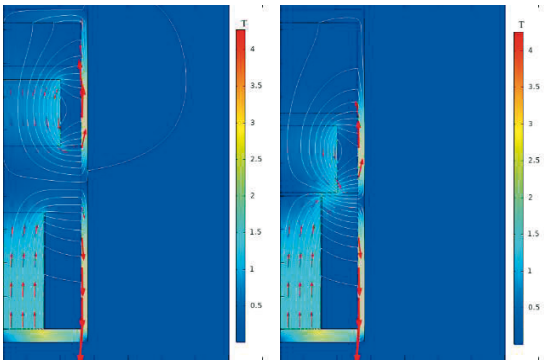

(d) h_1=35 mm (e) h_1=40 mm

Fig. 9 Magnetic field line distribution and magnetic induction intensity cloud diagram of the electromagnetic control unit for different heights of the permanent magnet 1

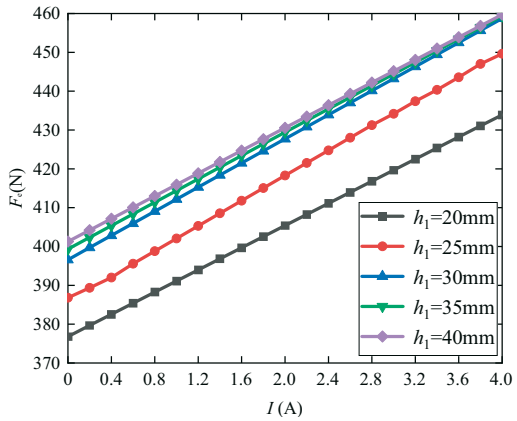

Fig. 10 The variation in the electromagnetic force with current for different heights of the permanent magnet 1

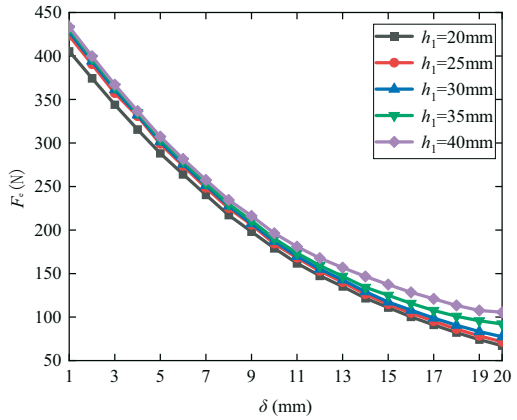

Fig. 11 The variation in the electromagnetic force with air gap for different heights of the permanent magnet 1

4. Electromagnetic force test

To assess the validity of the finite element model and evaluate the simulation analysis results, an electromagnetic force test system is constructed, as shown in Fig. 12. The permanent magnet 2 and permanent magnet 1 with coil are fixed to the base with a support. The gap (air gap δ) between the two permanent magnets can be controlled by adjusting the distance between the supports. The input current of the coil in the electromagnetic control units can be changed by the adjustable DC power supply, and the electromagnetic force acting on the permanent magnet 2 is input to the computer through the force sensor, digital transmitter, and USB-485 serial cable.

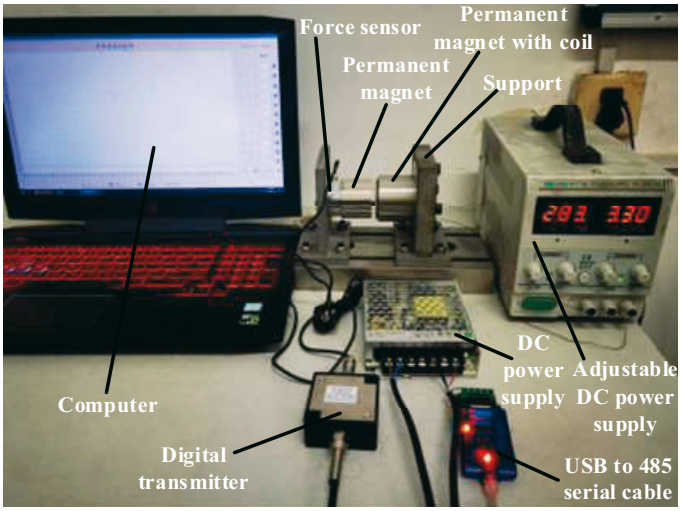

Fig. 12 A system for testing the electromagnetic force of the electromagnetic control unit

The electromagnetic force that acts on the permanent magnet 2under different air gaps is tested when the coil current is 0 A and 4 A. Figure 13 shows a comparison between the electromagnetic force test results and the simulation analysis results. The variation in the electromagnetic force with air gap obtained from the test and that from the simulation, both obtained under the same conditions, are similar. However, due to the existence of determining factors, such as part processing, test environment, geometric model simplification in the finite element analysis, grid size, and solution accuracy, there are also some differences between the actual electromagnetic force obtained from the test and that from the simulation. The maximum relative error between the two is 8.72%, which shows that the finite element simulation model of the electromagnetic field and the finite element analysis results of the electromagnetic control unit are effective.

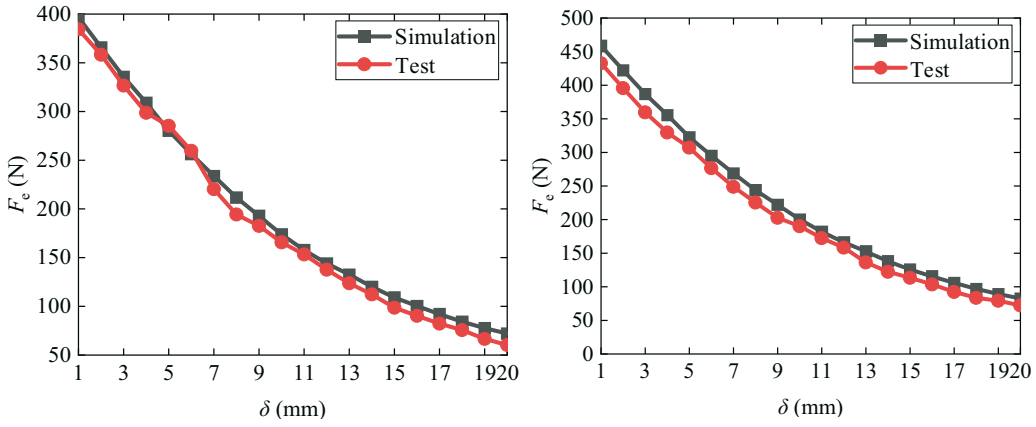

Fig. 13 Comparison between the results of electromagnetic force test and finite element simulation

5. Calculation of the moment of inertia

5.1 Force analysis

When the moment of inertia adjustment device works, the permanent magnet 2 and the short sleeve can slide along the long sleeve. Since multiple sets of electromagnetic control units installed on the moment of inertia adjustment device are evenly arranged relative to the rotational centre, the mechanical analysis of one set of the permanent magnet 2 and short sleeve in a single electromagnetic control unit is carried out. As shown in Fig. 14, point O is the rotational centre. The permanent magnet 2 and the short sleeve are regarded as a whole (as one moving mass), and the mass is set to be m. The stiffness and initial length of the spring are k and l_0, respectively. The distance from the spring attached to the primary flywheel to point O is r_0, and the distance from the centre of the moving mass to point O is r.

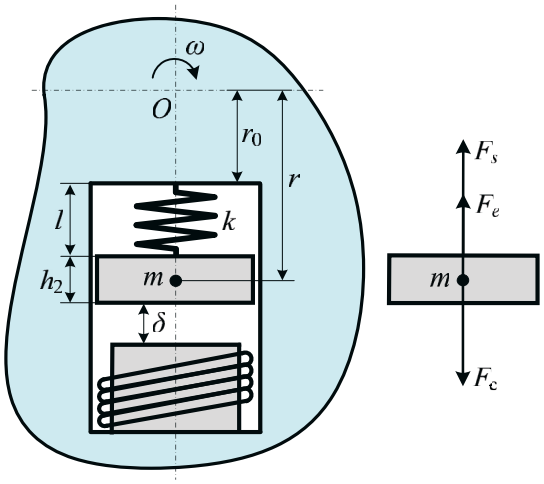

Fig. 14 Force analysis

The centrifugal force F_c of the moving mass is:

$$F_c = m\omega^2 r\,, \tag{1}$$

where ω is the rotational angular velocity.

When the spring deformation is Δl, the force F_s on the moving mass is:

$$F_s = k\Delta l\,. \tag{2}$$

During the movement of the moving mass, the air gap δ has the following relationship with the spring deformation Δl:

$$\delta = \delta_0 - \Delta l\,. \tag{3}$$

The length l of the spring after deformation under forces is:

$$l = l_0 + \Delta l\,. \tag{4}$$

The distance r from the centre of the moving mass to point O is:

$$r = r_0 + l + \frac{h_2}{2}\,. \tag{5}$$

After the speed of the device has stabilized, the following equation is obtained according to the force balance on the moving mass:

$$F_c - F_s - F_e = 0\,. \tag{6}$$

It is assumed that the relationship between the electromagnetic force and the air gap under the specific current of the coil conforms to the following formula [19]:

$$F_e = C_1\left(\frac{1}{C_2+\delta}\right)^2 + C_3\,, \tag{7}$$

where C_1, C_2, and C_3 are constants.

From equations (1) - (7), the following equation can be obtained:

$$\frac{m\omega^2}{C_1}\left(r_0 + l_0 + \frac{h_2}{2}\right) + \frac{m\omega^2 - k}{C_1}\Delta l - \frac{C_3}{C_1} = \left(\frac{1}{C_2 + \delta_0 - \Delta l}\right)^2. \tag{8}$$

Nonlinear fitting is performed on the data obtained from the finite element simulation analysis of electromagnetic force when the coil current I is equal to 4 A, as shown in Fig. 15. Under this condition, C_1=0.1162, C_2=0.01439, and C_3=0.

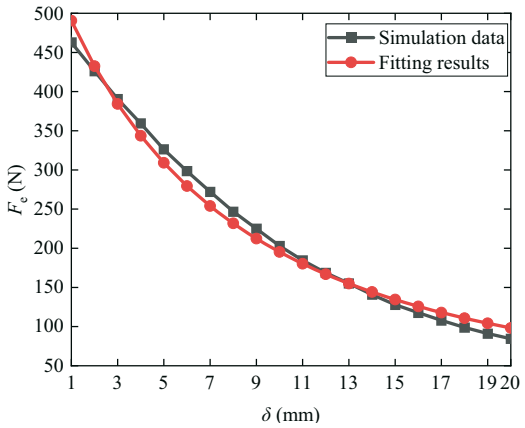

Fig. 15 Non-linear fitting of electromagnetic force simulation data when I=4 A

5.2 Calculation of the moment of inertia

According to the parallel axis theorem of the moment of inertia, the moment of inertia of a single permanent magnet 2 and a short sleeve around the rotational centre can be expressed as:

$$J_m = \frac{1}{12}m\left(\frac{3}{4}d_2^{\,2} + h_2^{\,2}\right) + mr^2\,. \tag{9}$$

There are four sets of electromagnetic control units. Thus, the total moment of inertia can be expressed as:

$$J = J_u + 4J_m\,, \tag{10}$$

where J_u is the inertia expression of the immutable part in the structure.

In the electromagnetic control unit, the mass m of the moving mass is 0.3 kg, the stiffness of the spring k is 20 N/mm, r_0=35 mm, l_0=50 mm, and the original inertia expression of the immutable part J_u is 0.01 kg·m^2. According to the above analysis, the relationship between the moment of inertia of the device and the rotation speed can be obtained when the input current of the coil is taken to be 0 A, 6 A, and 12 A, respectively, as shown in Fig. 16.

As the rotation speed increases, the moment of inertia of the structure also increases. Until the moving mass reaches the limit position, the moment of inertia remains unchanged as the rotation speed continues to increase. However, the minimum value of the moment of inertia is different for different currents. The main cause of this is that the electromagnetic force acting on the moving mass is different even at a speed of 0 r/min for different currents, and, therefore, the spring deformation Δl is also different. As the speed increases, the influence of the current on the moment of inertia becomes stronger because, at low speed, the centrifugal force is small, the air gap δ is large, and the influence of the current on the electromagnetic force is small. In addition, the minimum and maximum moments of inertia of the structure are 0.0203 kg·m^2 and 0.0262 kg·m^2, respectively. The maximum adjustable proportion of the moment of inertia of the structure can reach 29.06%.

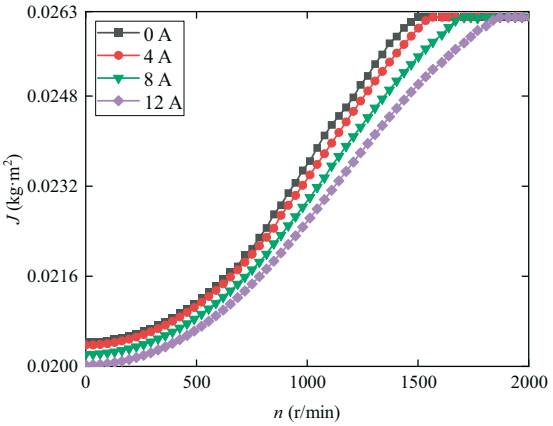

Fig. 16 The variation in the moments of inertia with speed at different currents

6. Conclusions

(1) A moment of inertia adjustment device based on electromagnetic control is proposed. The finite element simulation analysis model of the electromagnetic control unit is established. The influence of materials and structure parameters of the electromagnetic control unit on the electromagnetic field is analysed.

(2) The electromagnetic force test system of the electromagnetic control unit is designed and constructed. The results of the electromagnetic force test are close to the results of the finite element simulation analysis, which confirms the accuracy and effectiveness of the simulation model.

(3) The force analysis of the electromagnetic control unit is carried out, and the formula of the moment of inertia is devised. The variation in the moment of inertia of the device under different speeds and currents is discussed. The results show that the proposed moment of inertia adjustment device can be used to finely adjust the moment of inertia. The maximum adjustable proportion of the moment of inertia of the device can reach 29.06%. This study provides a reference for better control of vibrations in rotor systems.

Acknowledgements

This study was supported by the National Natural Science Foundation of China (Grant Nos. 51805167 and 52265011), the Natural Science Foundation of Jiangxi Province (Grant No. 20232BAB204044), the Foundation of Educational Department of Jiangxi Province (Grant No. GJJ2200624), and the Key Scientific Research Projects of Colleges and Universities of Henan Province (Grant No. 23B460007)

REFERENCES

[1] Bolund, B.; Bernhoff, H.; Leijon M. Flywheel energy and power storage systems. Renew Sustain Energy Rev, 2007, 235–258, 11(2). https://doi.org/10.1016/j.rser.2005.01.004
[2] Christopher, D. A.; Beach, R. Flywheel technology development program for aerospace applications. IEEE Aerosp Electron Syst Mag, 1998, 13(6): 9–14. https://doi.org/10.1109/62.683723
[3] Su, N. Q.; Zhang, Q. H. Chen, Y. D.; Chang, X. X.; Liu, Y. Composite Fault Diagnosis in Rotating Machinery Based on Multi-Feature Fusion. Transactions of FAMENA, 2024, 01: 87-96. https://doi.org/10.21278/TOF.481054223
[4] Filipović, I.; Bibić, D.; Milašinović, A.; et al. Preliminary selection of basic parameters of different torsional vibration dampers intended for use in medium-speed diesel engines. Transactions of FAMENA, 2012, 36(3): 79-88. https://hrcak.srce.hr/89243
[5] Li, S.; Zheng, L. Vibration Attenuation Mechanism of the Rotor System with Anisotropic Support Stiffness. Transactions of FAMENA, 2021, 45(1): 129-144. https://doi.org/10.21278/TOF.451017220
[6] Fu, Z. J.; Zhang, X. Zhang, Z. G.; Zhao, D. F.; Yin, Y. A Review on Modeling and Control of Magnetorheological Dampers. Transactions of FAMENA, 2024, 03: 53-76. https://doi.org/10.21278/TOF.483061123
[7] Yang, S.; Xu. T.; Li. C.; Liang, M.; Baddour, N. Design, Modeling and Testing of a Two-Terminal Mass Device with a Variable Inertia Flywheel. Journal of Mechanical Design, 2016, 138(9): 095001. https://doi.org/10.1115/1.4034174
[8] Ullman, D. G. A variable inertia flywheel as an energy storage system. The Ohio State University, 1978.
[9] Van de, V. J. D. Fluidic variable inertia flywheel and flywheel accumulator system. U.S. Patent, US2012011960A1.
[10] Dugas, P. J. Variable inertia flywheel. U.S. Patent, US20150204418A1.
[11] Jayakar, V.; Das, Sumit K. Variable inertia flywheel. U.S. Patent, US20120291589A1.
[12] Xu, T.; Liang. M.; Li. C. Design and analysis of a shock absorber with variable moment of inertia for passive vehicle suspensions. Journal of Sound and Vibration, 2015, 355:66–85. https://doi.org/10.1016/j.jsv.2015.05.035
[13] Kondoh, J.; Funamoto, T.; Nakanishi, T.; Arai, R. Energy characteristics of a fixed-speed flywheel energy storage system with direct grid-connection. Energy, 2018, 165: 701–708. https://doi.org/10.1016/j.energy.2018.09.197
[14] Kushwaha, P.; Ghoshal, S K.; Dasgupta, K. Dynamic analysis of a hydraulic motor drive with variable inertia flywheel. Proceedings of the Institution of Mechanical Engineers Part I: Journal of Systems and Control Engineering, 2019, 234(6): 734–747. https://doi.org/10.1177/0959651819875914
[15] Zhang, Y.; Zhang, X.; Qian, T.; et al. Modeling and simulation of a passive variable inertia flywheel for diesel generator. Energy Reports, 2020, 6: 58–68. https://doi.org/10.1016/j.egyr.2020.01.001
[16] Su, H. K.; Liu, T. Design and analysis of hybrid power systems with variable inertia flywheel. World Electric Vehicle Journal, 2010, 4(3): 452–459. https://doi.org/10.3390/wevj4030452
[17] Harrowell, R. V. Elastomer flywheel energy store. International Journal of Mechanical Sciences, 1994, 36(2):95–103. https://doi.org/10.1016/0020-7403(94)90078-7
[18] Chen, P.; Yang, Y. Design, Dynamics Modeling, and Experiments of a Vibration Energy Harvester on Bicycle. Transactions on Mechatronics, 2023, 28(5), 2670–2678. https://doi.org/10.1109/TMECH.2023.3246516
[19] Chen, H. X.; Li, Y. G.; Long, Z. Q.; Chang, W.S. Optimal design and characteristic analysis of hybrid magnet in maglev system. Journal of System Simulation, 2010, 22(4), 837–840. https://doi.org/10.16182/j.cnki.joss.2010.04.023

Submitted: 12.12.2023
Accepted: 11.02.2025

Liping Zeng*
Zihao Wan
Gang Li
Ruqi Ding
Guoliang Hu
School of Mechatronics and Vehicle Engineering, East China Jiaotong University, Nanchang, China
Hongen Niu
College of Mechanical and Electronical Engineering, Zhengzhou University of Industrial Technology, Xinzheng, China
*Corresponding author:
melpzeng@163.com